CHALMERS
UNIVERSITY OF TECHNOLOGY

Reinforcement learning-based event-triggered secondary control of DC microgrids

Energy Reports 11 (2024) 2818–2831

Contents lists available at ScienceDirect

Energy Reports

journal homepage: www.elsevier.com/locate/egyr

Research paper

Reinforcement learning-based event-triggered secondary control of DC microgrids

Houshmand Negahdar [a], Amin Karimi [a,*], Yousef Khayat [b,**], Saeed Golestan [c]

[a] Dept. of Electrical Engineering, IAU, Sanandaj Branch, Sanandaj, Iran
[b] Dept. of Electrical Engineering, Chalmers University of Technology, Göteborg, Sweden
[c] AAU Energy, Aalborg University, DK-9220 Aalborg, Denmark

ARTICLE INFO

Keywords:
Artificial intelligent
DC microgrids
Event-triggered control
Power-sharing
Reinforcement learning
Secondary control
Voltage regulation

ABSTRACT

In this paper, a reinforcement learning (RL)-based event-triggered mechanism (ETM) for employing in the secondary control layer (SCL) of DC microgrids is developed. The proposed RL-based ETM satisfies the SCL objectives, which is overcoming the disadvantages of primary control (such as voltage deviation and inappropriate current sharing among the distributed generating units). More importantly, it also aids in reducing the amount of transmitted data exchanged within all the distributed generators (DGs). The design parameters of the ETM scheme are regulated through a robust RL approach to provide adaptive ETM parameter tuning, enabling the ETM error vector threshold to quickly adapt to changes in the MG. The suggested RL-based ETM approach is implemented in a DC microgrid, and utilizing hardware in the loop (HIL) real-time OPAL-RT experimental tests, its performance in the SCL of DC microgrids is investigated. Experimental validations have confirmed the merits of the proposed approach.

1. Introduction

The increasing integration of renewable energy sources (RESs) and energy storage systems (ESSs) presents critical challenges for system stability. Microgrids (MGs) have emerged as a solution, offering a framework for integrating RESs, ESSs, and controllable loads into compact networks. These networks can be configured as DC, AC, or hybrid systems. Microgrids provide several advantages, including enhanced reliability, scalability, flexibility, and efficiency (Barone et al., 2023). These benefits are often hard to attain in traditional power systems. In addition to these features, the compatibility of DC microgrids with DC-powered RESs, ESSs, and electronic loads, such as electric vehicles and data centers, is particularly advantageous for industrial applications. Furthermore, DC microgrids are free from issues related to reactive power, harmonics, and synchronization problems, and they benefit from simpler control systems. These advantages collectively contribute to lower development, implementation, and operational costs, making DC microgrids a compelling alternative to AC microgrids for practical applications (Chen et al., 2022).

In autonomous mode, the MG operates independently, making the control structure crucial for ensuring stability and preventing abnormal operation (Fathollahi et al., 2023). Typically, DC MGs employ a hierarchical control structure to achieve control objectives, consisting of primary, secondary, and tertiary control layers. The secondary control level (SCL) in DC MGs primarily focuses on voltage regulation (VR) and accurate Load-sharing (LSH). Various strategies, particularly hierarchical control, have been explored in the literature to meet these objectives (Naderi et al., 2023). The VR and LSH are controlled based on local measurements through a conventional droop control loop. However, the inherent function of the droop mechanism leads to voltage deviation and inadequate LSH at the primary level. These issues can be effectively addressed using secondary control, which has architectures that can be classified into centralized, decentralized, and distributed, based on the communication perspective (Moradi et al., 2023; Khayat et al., 2019).

In the centralized SC architecture, traditionally seen as the conventional solution, there is a significant computational burden, as it requires simultaneous access to all necessary DGUs' information. Additionally, this architecture lacks straightforward scalability and is vulnerable to a single point of failure. In contrast, the decentralized SC scheme relies on local controllers to perform VR and LSH. These controllers often use complicated, estimation-based, or other time-consuming approaches without relying on a communication infrastructure (Nikoobakht et al., 2022; Vafamand et al., 2023). However, their responses are often not accurate or fast enough to meet the secondary control objectives (Sepehrzad et al., 2023). Distributed SCs, on

* Corresponding author.
** Corresponding author.
E-mail addresses: a.karimi@iausdj.ac.ir (A. Karimi), yousefkh@chalmers.se (Y. Khayat).

https://doi.org/10.1016/j.egyr.2024.02.033
Received 26 November 2023; Received in revised form 9 February 2024; Accepted 18 February 2024
Available online 26 February 2024

Nomenclature

MG	Microgrid
RL	Reinforcement learning
ETM	Event-triggered mechanism
SCL	Secondary control layer
CI	Communication infrastructure
DG	Distributed generation
HiL	Hardware-in-the-loop
RES	Renewable energy sources
ESS	Energy storage systems
VR	Voltage regulation
LSH	Load-sharing
CC	Current controller
VC	Voltage controller
DCA	Dynamics consensus algorithm
PnP	Plug and play
SI	Sensory input
ES	Emotional signal
LPF	Low-pass filter
MAS	Multi-agent system
BW	Bandwidth
PCC	Point of common coupling
SF	Scaling factor
LBCL	Low bandwidth CI

Variables

L_i	Converter's input inductor
r_i	Input inductor's resistance
C_i	Converter's output capacitor filter
L_{linei}	Line's inductor
R_{Linei}	Lines's resistance
α_{ij}	Communication's coupling gain
δu_i	SCL's correction term
$x_i(t)$	State variable
N	Number of MG's DGUs
$\mathcal{G}_r$	MG's communication digraph
$V_{\mathcal{G}}$	Set of nodes of $\mathcal{G}_r$
$E_{\mathcal{G}}$	Set of the edges of nodes of $\mathcal{G}_r$
$A_{\mathcal{G}}$	Adjacency matrix for the CI $\mathcal{G}_r$
$\lambda_1(\mathcal{G})$	Laplacian's eigenvalue of the $\mathcal{G}_r$
d_{ci}	Control effort of the CC
k_{pi}	Proportional gain of the CC
k_{ii}	Integral gain of the CC
k_{pv}	Proportional gain of the VC
k_{iv}	Integral gain of the VC
v_{MG}	Nominal voltage of the MG
n_{di}	DGU_i's droop gain
$u_i(t^i_k, t^j_k)$	Sampled control signal
t^i_k , t^j_k	ETM instants for two neighbor DG
ε_i	ETM positive term to avoid Zeno
ϑ_i	ETM disturbance mitigation gain
κ_i	ETM state derivative reduction rate

the other hand, are widely recognized for improving MGs' stability and scalability (Moradi et al., 2023), thanks to the fewer communication links they require.

The data exchange mechanism in the SCL has not yet been adequately addressed in the literature. It is recognized as a major challenge that can affect system stability due to time delays, measurement noise, cyber uncertainties, disturbances, and limited communication-layer bandwidth (Moradi et al., 2024). Conventionally, data exchange among DGUs involves a periodic sampling and transmitting mechanism at predefined intervals, known as 'time-triggered' data exchange (Peng et al., 2020b). In such a scheme, DGUs continuously exchange information, even in steady-state conditions. This approach requires higher bandwidth in the communication layer and imposes a heavier load on the communication networks (Najafirad et al., 2023).

Due to the limited bandwidth in the SCL of MGs (Ansari et al., 2022), it is necessary to minimize traffic in communication channels to avoid overuse and overcrowding of bandwidth, especially when transmitting non-essential redundant data. This is particularly important during situations where multiple control objectives need to be managed through the cyber layer (Wang et al., 2021b). Note that overuse of bandwidth can lead to increased delays and packet losses during data exchange, which in turn affects system stability and reliability (Naderi et al., 2021; Afshari et al., 2021). To address these issues, aperiodic data exchange mechanisms like event-triggered mechanisms (ETM) have been recently proposed for use in the cyber layer (Li et al., 2022).

ETMs are introduced as a promising method to mitigate over-usage of the communication layer in multi-agent systems, particularly in DC MGs (Fan et al., 2019). A dynamic ETM-based SC with decentralized detectors for DC MGs was presented in Lu et al. (2021), Jamali et al. (2023), which, due to its detector mechanism, requires continuous monitoring of other DGUs and exhibits some disadvantages of centralized control. A distributed ETM presented in Alavi et al. (2018) aimed to address these issues, but it lacks flexibility in adapting to system mode changes and is prone to Zeno behavior, which are significant drawbacks. The leader–follower ETM, developed using a robust sliding-mode concept, was introduced in Jamali et al. (2023), and a robust H_∞ ETM approach for enhancing system stability against uncertainties was proposed in Zhou et al. (2019). Despite these advancements, cyber uncertainties or defects in the leader unit can still compromise system stability. In Wang et al. (2021a), Qian et al. (2022), leader–follower ETM mechanisms are considered, although they suffer from a slow dynamic response, which is a notable limitation.

In Shafiee et al. (2021), an advanced nonlinear ETM is proposed, featuring state-dependent tolerance and a positive threshold. However, determining the stable range for design parameters is complex, representing its main drawback. In Peng et al. (2020a), an ETM strategy is introduced that utilizes the latest data exchanged among DGUs with varying line impedance. Its shortcomings are evident in its poor dynamic performance during Plug-and-Play (PnP) operations and reduced effectiveness during communication link failures. Furthermore, Fan et al. (2019) presents a discrete-time ETM, which checks the error threshold at specific sampling times in a distributed manner. Despite its innovative approach, it struggles with a lack of adaptability to changes in system operations. This technique becomes overly complex as the number of DGUs in the MG increases. Another discrete ETM, discussed in Khalili et al. (2022), aims to address the LSH problem while employing a decentralized mechanism for VR. However, its effectiveness has not been evaluated in various scenarios, such as DGU's PnP functionality and link failure studies. The authors in Shi et al. (2020) propose an optimization-based ETM as a solution to fulfill the primary objectives of DC MGs, enhancing system resiliency. Lastly, an ETM proposed in Du et al. (2023) focuses on improving system performance under denial-of-service cyber-attacks.

Time delays for ETM scheme are also recently been considered in Yan et al. (2022) for load frequency control of power systems with high penetration of wind power plants. To deal with the control saturation issues of linear systems subject to mixed delay concerns, in Yan et al. (2023b) a polytopic representation is employed to cope with the nonlinear saturation unit, which leads to ensuring the system stability. In this line, authors in Yan et al. (2023a) a weighted memory H_∞ controller for time-varying delays based on instantaneous historical

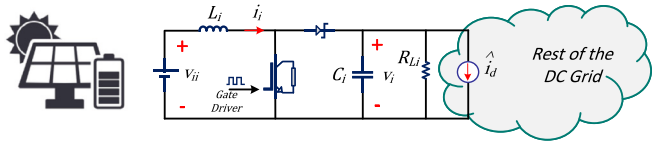

Fig. 1. General Configuration of a DC–DC boost power converter for DC MG applications.

data over a given period is provided to construct a fuzzy-based memory controller.

This study presents an RL-based ETM for the dynamic consensus algorithm (DCA) in the SCL of DC MGs. This mechanism aims to fulfill the primary objectives of the SCL while minimizing data exchange. It allows each DGU to independently decide when to exchange data with others. There was no appropriate performance index to tune those parameters. Unlike Shafiee et al. (2021), a different Zeno free feature is developed according to the consensus dynamics of the system. In addition, since there was no appropriate performance index to tune ETM parameters in Shafiee et al. (2021), by employing the proposed RL-scheme and the provided cost function in the current work, an appropriate performance index for tuning the parameters are determined subjected to accurate load sharing among the units. The performance of the proposed RL-based ETM is compared with the base ETM, and the influence of the RL unit on the performance and event instants is depicted. The distributed predefined-time optimization approach presented in Wang et al. (2024) has developed a multi-objective optimization problem with penalty factors for presenting the global optimal solution, which is realized through a time-dependent function and a distributed predefined-time observer. Unlike the developed optimization-based solution (Wang et al., 2024), which relies on a predefined algorithm, fixed parameters, and knowledge about system configuration and grid conductance matrix, the proposed RL-based ETM offers adaptability and learning capabilities in dynamic environments for ETM parameter tuning. The other key features of the proposed ETM include:

- **System Stability:** The RL-based ETM maintains system stability and achieves all SCL goals. The adaptive component of RL is tasked with tuning ETM parameters, while the ETM itself determines the optimal moments for data exchange among DGUs to meet the SCL objectives in DC MGs
- **Reduced Data Exchange:** The RL-based ETM significantly decreases the volume of data exchanged through the communication infrastructure. This leads to the attainment of SCL objectives with fewer data transmissions, thereby requiring less communication bandwidth.
- **Design and Verification:** The design and verification of the ETM are straightforward and real-time, allowing for the selection of appropriate parameters under different operating conditions of a DC MG. The implementation follows a step-by-step approach, utilizing brain-emotional RL to manage voltage restoration and power-sharing in DC MGs.

The remaining parts of this paper are organized as follows: Section 2 presents a comprehensive modeling scheme of the system, including cyber layer notation and description, control loops, and the physical dynamics of the power converters. Section 3 details the proposed RL-based ETM design procedure. The effectiveness of the proposed RL-based ETM scheme is then investigated through experimental tests in Section 4. Finally, concluding remarks are provided in Section 5.

2. Model description of the system

A DC MG is an integration of physical and cyber layers. The physical layer of a DC MG includes DC–DC power converters, which are used for transmitting the electric power from the prime mover side toward the network side through electrical lines. The cyber layer is a sparse net that modifies the DGU dynamics by exchanging information. This section goes over the definitions of graphs and required differential equations for modeling the system dynamics.

2.1. Boost converter model

A boost power converter with the common model illustrated in Fig. 1 is employed in DG_i of the considered DC MG system. Where v_{ii} and v_{io} are the input and output voltages, respectively. L_i, r_i, C_i, L_{linei} and R_{Linei} are the input inductor, output capacitor filter, resistance of the input inductor and output capacitor, respectively. By using the circuit laws, differential equations to derivate state space representation can be represented as

$$\begin{bmatrix} \dot{i}_i \\ \dot{v}_i \end{bmatrix} = \begin{bmatrix} 0 & -\frac{(1-d)}{L_i} \\ \frac{(1-d)}{C_i} & -\frac{1}{R_{Li}C_i} \end{bmatrix} \begin{bmatrix} i_i \\ v_i \end{bmatrix} + \begin{bmatrix} -\frac{1}{L_i} & 0 \\ 0 & -\frac{1}{C_i} \end{bmatrix} \begin{bmatrix} v_{ii} \\ \hat{i}_d \end{bmatrix} \tag{1}$$

where d is the control effort or the duty cycle generated by the gate driver. L_i, C_i, and R_{Li} stand for the input inductance, output capacitance, and the local load, respectively. i_i, v_i, d, v_{ii}, and $\hat{i}_d$ are the input inductance current as the first state variable, output voltage as the second state variable, input voltage, and the perturbed current from the rest of the DG units, as scrutinized in Batmani et al. (2022).

2.2. Cyber layer model

The communication network, in the suggested mechanism, needs to be in the form of a bidirectional graph. In this way, DGUs can be considered as nodes, and their communication links as edges. On the basis of a graph, communication networks can be expressed as

$$\mathcal{G}_r = (V_\mathcal{G}, E_\mathcal{G}, A_\mathcal{G}) \tag{2}$$

in which

$$V_\mathcal{G} = (v_1, v_2, \ldots, v_N), E_\mathcal{G} \subset V_\mathcal{G} \times V_\mathcal{G} \tag{3}$$

stands for a limited but non-zero set of N nodes and the set of the edges or the communication links. In addition,

$$A_\mathcal{G} = [a_{ij}] \in R^N \times R^N$$

expresses the adjacency matrix for the cyber-connected agents. The transmitted weighted data between ith DGU and the jth DGU can be expressed as a_{ij}. In case of the ith DGU and the jth DGU are linked for exchanging data shown by an edge, then $a_{ij} > 0$, otherwise $a_{ij} = 0$.

The neighbors set for ith DGU is here shown by N_i. In the case of $j \in N_i$, then jth DGU is able to send its information toward the ith DGU. $D = diag\{d_i\}$ is introduced as a diagonal matrix and generally is entitled as an "in-degree, out-degree" matrix to show the number of neighbors of a specific DGU, where $d_i = \Sigma_{j \in N_i} a_{ij}$.

$\mathcal{G}_r$ is determined as an "undirected" graph in case the communication links can be expressed as bidirectional. In this case, $\forall i, j$, the term

$$(v_i, v_j) \in E_\mathcal{G} \Leftrightarrow (v_j, v_i) \in E_\mathcal{G}$$

can be always held. In this situation, the mentioned graph has always a symmetric Laplacian matrix representation as $L = D - A$, due to the fact that the algebraic sum of each row (column) of Laplacian matrices equals zero. Therefore, all undirected graphs have a zero eigenvalue. The Laplacian's eigenvalues can easily determine the system's general dynamics, which can be denoted as

$$0 = \lambda_1(\mathcal{G}) \leq \lambda_2(\mathcal{G}) \leq \ldots \leq \lambda_N(\mathcal{G})$$

At last, agents in a cyber–physical system can be considered as strongly connected units, in case there exists a path that connects any two unique nodes (Guo et al., 2019).

2.3. Control layers model

The DC-DC converters in the studied DC MG have been equipped with the primary and secondary control loops, as also shown in Fig. 2. Conventional proportional–integral (PI) controllers are considered for the inner voltage and current loops of the DC–DC converter, as

$$d_{ci} = (k_{pi} + k_{ii}/s) \times (i_{refi} - i_{oi}) \tag{4}$$

where d_{ci}, k_{pi}, k_{ii} stand for the control effort of the current controller, proportional, and integral coefficient of the current controller, respectively. i_{refi}, and i_{oi} are the reference currents generated by the voltage controller and the measured current of the boost power converter. The reference-generated current is given by

$$i_{refi} = (k_{pv} + k_{iv}/s) \times (v_{refi} - v_{dci}) \tag{5}$$

where k_{pv}, and k_{iv} are the proportional, and integral coefficients of the voltage controller, respectively. v_{refi} expresses the regulated voltage by the droop controller, which is adjusted through

$$v_{refi} = v_{MG} - n_{di} i_{oi} \tag{6}$$

where v_{MG} and n_{di} denote nominal voltage of the MG, and the droop coefficient value.

In the cyber layer, one can formulate the dynamics consensus algorithm (DCA) as

$$\dot{\bar{x}}_i(t) = \dot{x}_i(t) + u_i(t) \tag{7}$$

where

$$\bar{x}_i(t) = [\bar{v}_i, \bar{i}_{i(pu)}] \in \mathbb{R}^{N\times 2}$$
$$x_i(t) = [v_{dci}, i_{oi(pu)}] \in \mathbb{R}^{N\times 2}$$
$$u_i(t) = [u_{\hat{v}_i}, u_{\hat{i}_{i(pu)}}] \in \mathbb{R}^{N\times 2}$$

denote the dynamic averaged for the states of the ith unit, measured states, and inputs for the controller, respectively. Mostly, $u_i(t)$ can be expressed in the form of

$$\begin{cases} \dot{x}_i(t) = -\alpha x_i(t) - \beta \Sigma_{j\in N_i} a_{ij}(\hat{u}_i(t) - \hat{u}_j(t)) \\ u_i(t) = -C \sum_{j\in N_i} a_{ij} \left(\hat{x}_i(t_k^i) - \hat{x}_j(t_k^j)\right) \end{cases} \tag{8}$$

where $\hat{x}_i(t_k^i)$ and $\hat{x}_j(t_k^j)$ represent the last transmitted data to/from the neighbors of the ith DGU. Furthermore, $C \in [\ c_v\ c_{\bar{i}}\ ]$, where c_v and $c_{\bar{i}}$ represents positive convergence rate gains for the voltage DCA and current DCA, respectively. The minimum value of these gains can be considered to one. Substituting (8) in (7) results in the following formulation for DCA of the voltage and current

$$\dot{\bar{v}}_i(t) = \dot{v}_{dci}(t) - c_v \sum_{j\in N_i} a_{ij} \left(\hat{v}_i(t) - \hat{v}_j(t)\right) \tag{9}$$

$$\dot{\bar{i}}_{i(pu)}(t) = \dot{i}_{oi(pu)}(t) - c_{\bar{i}} \sum_{j\in N_i} a_{ij} (\hat{i}_{i(pu)}(t) - \hat{i}_{j(pu)}(t)) \tag{10}$$

where $i_{oi(pu)} = i_{oi}/i_{i,\max} i_{oi} i_{i,\max}$.

As it can be observed from Fig. 2, the correction term generated by the DCA in the SC layer, *i.e.*, $\delta = \delta_v + \delta_i$, is added to the droop control loops for compensating the induced voltage drop as

$$v_{refi} = v_{MG} - n_d i_{oi} + \delta_v + \delta_i \tag{11}$$

By this way, the DCA of the voltage and current objectives are provided to realize the convergence of average voltage of DGUs to the V_{MG}, and convergence of per-unit value of the currents of each DGU to the averaged per-unit current of DGUs. As shown in Fig. 2, in this paper, $[\hat{v}_i \hat{i}_{i(pu)}]$ for each unit are calculated by the ith DG's ETM unit, and $[\hat{v}_j \hat{i}_{j(pu)}]$ are calculated first by the jth DG's ETM unit and then they are transmitted by the sampled communication network.

3. Proposed intelligent BEL event mechanism

In this section, The proposed RL-based ETM technique according to the voltage and current DCAs is first developed. Then, the application of the proposed intelligent BEL technique for the optimal regulation of the Lyapunov control is employed. The design procedure begins with a deriving a Lyapunov control law for the ETM, and then through the performance analysis, the regulation procedure is conducted to establish the initial adjustments for the gains. Following this, the BEL method is implemented to facilitate precise real-time adaptation of the control gains.

3.1. Step I: ETM principle

To determine the control law and update the inter-event times, the control input is first computed according to the last sampled data exchanged among the DGUs during the error times. The sample remains fixed as long as it needs to be updated when the error passes the threshold. To do this, the sampled control signal is defined as $u_i(t) = u_i(t_k^i, t_k^j)$, such that

$$u_i(t_k^i, t_k^j) = -C \sum_{j\in N_i} a_{ij}(\hat{x}_i(t_k^i) - \hat{x}_j(t_k^j)),\ \forall\ t\ \in\ [t_k^i,\ t_{k+1}^i) \tag{12}$$

where t_k^i and t_k^j stand for the event triggered instants among the ith DGU and its cyber neighbors. By using the Laplacian matrix, defined in Section 2.2, (12) can be rewritten as

$$u(t_k^i, t_k^j) = -CL\hat{x}(t_k^i, t_k^j). \tag{13}$$

One can utilize the derivation of the measured states as disturbance, (*i.e.*, $\psi(t) = \dot{x}(t)$). Therefore, (7) can be reformulated as

$$\dot{\bar{x}}(t) = \psi(t) - CL\hat{x}(t_k^i, t_k^j) \tag{14}$$

Now, in order to determine the error signal, one can utilize a sample and hold (S/H) block. To do so, a signal being given into a S/H block, and an error term can be generated by comparing the sampled data with the input signal. Considering this, the error for the ith DGU, as the deviation between the averaged signal, which also is a continuous signal, and its S/H form at the event time, can be formulated as

$$e_i(t) = \hat{x}_i(t_k^i, t_k^j) - \bar{x}_i(t). \tag{15}$$

It should be highlighted that the updating times instants $\{t_k^i\}$ have to be calculated such that the system keeps its stability. The mentioned instants can be defined as

$$t_{k+1}^i = \inf\{t > t_k^i\ :\ \|e_i(t)\| > \kappa_i \|\hat{z}_i(t_k^i, t_k^j)\| + \vartheta_i \|\psi_i(t)\| + \varepsilon_i\} \tag{16}$$

where $\inf\{\cdot\}$ and $\|\cdot\|$ are used to show the infimum of a signal and Euclidean norm (for vectors), respectively. ε_i represents design positive terms to avoid occurring the Zeno phenomenon. Both the ϑ_i, and κ_i are design parameters which represent disturbance mitigation and state derivative reduction rate for Lyapunov design, which can be systematically tuned, as it will be provided later. $\hat{z}_i$ is the disagreement value among the ith DGU and its cyber neighbors. In addition, the derivation of the measured states ψ_i is employed in the threshold ton increase the adaptive disturbance rejection and improves the robustness of the system. ε_i in (16) forbids occurring Zeno phenomenon by giving a small bound for the error growth.

As it can be inferred from (16), a new update is necessitated to update the control signal recalculation according to the exchanged data, as long as $\|e_i(t)\|$ surpasses its pre-defined threshold. Otherwise, the condition is then no longer going to be triggered by small error, and thus, Zeno behavior does not occur. The provided ETM scheme implementation is shown in Fig. 2, where, the latest sampled-data is exchanged among the neighbors of unit i, whenever the considered error threshold is touched in the location of the unit i; otherwise, the control signal keeps calculating the regulation law by the previous form of the received data.

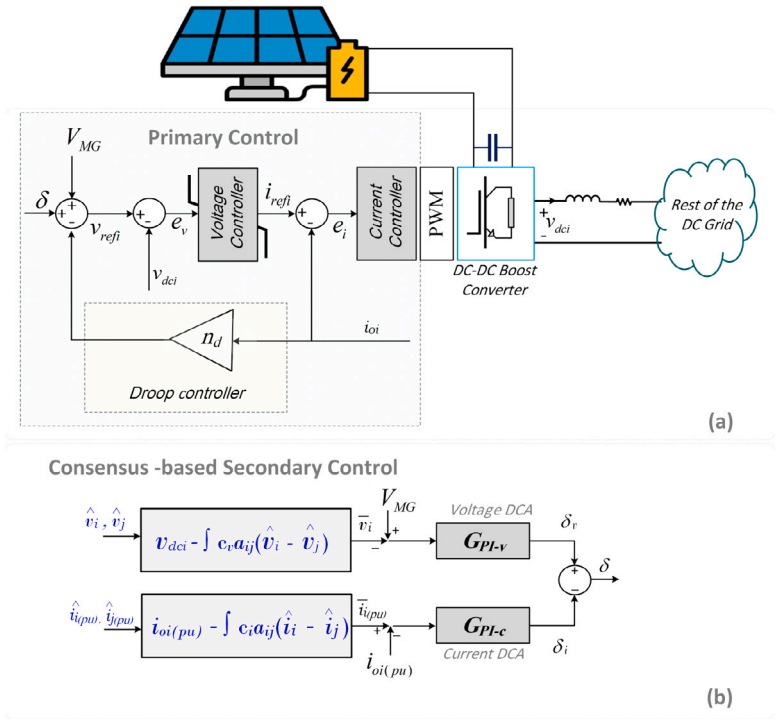

Fig. 2. Physical structure and control layers of a DC power converter in a DC grid. (a) The architecture of current, voltage, and droop controller with the correction term δ from the secondary control loop. (b) The conventional consensus secondary control scheme for generating the secondary correction term δ by the current and voltage DCAs.

3.1.1. ETM parameter design

To show the design criteria for the ETM parameters. Through a Lyapunov-based design procedure, the feasible bounds for guaranteeing the stability of the control system can be derived. To form the regulation law to design the controller gains and ETM parameters, let us first consider

$$\mathcal{V}(\bar{x}(t)) = (\bar{x}^T(t) L \bar{x}(t))/2 \tag{17}$$

as a candidate for Lyapunov function for evaluating the system stability. By time derivating of both the sides of the Lyapunov candidate as $\dot{\mathcal{V}}(\bar{x}(t)) = \bar{x}^T(t) L \dot{\bar{x}}(t)$, and employing (14) one can reformulate the time derivative of the Lyapunov candidate as

$$\dot{\mathcal{V}}(\bar{x}(t)) = \bar{x}^T(t) L \psi(t) - C \bar{x}^T(t) L L \hat{x}(t_k^i, t_k^j). \tag{18}$$

By assuming that the continuous access to the data of the cyber neighbors is infeasible, and the latest S/H data can be employed in the analysis stage of the Lyapunov candidate, the possible range of the design parameters can be achieved. To this aim, $\bar{x}(t)$ is replaced with $\hat{x}(t_k^i, t_k^j) - e_i(t)$, and by defining $\hat{z}(t_k^i, t_k^j) = L\hat{x}(t_k^i, t_k^j)$. Therefore, (18) can be reformulated as

$$\begin{aligned}\dot{\mathcal{V}}(\bar{x}(t)) = &-C\hat{z}^T(t_k^i, t_k^j)\hat{z}(t_k^i, t_k^j) + \hat{z}^T(t_k^i, t_k^j)\psi(t) \\ &-(Le(t))^T\psi(t) + C(Le(t))^T\hat{z}(t_k^i, t_k^j).\end{aligned} \tag{19}$$

By breaking (19) into its Sigma form, and thanks to the fact that the CI has been assumed as a symmetric graph, (19) can be represented to

$$\begin{aligned}\dot{\mathcal{V}} = &-C\sum_i \hat{z}_i^2 + C\sum_i |N_i|\,\hat{z}_i e_i + \sum_i \hat{z}_i\psi_i + C\sum_{i,j\in N_i}\hat{z}_i\,(-e_j) \\ &+\sum_i |N_i|\,\psi_i\,(-e_i) + \sum_{i,j\in N_i}\psi_i e_j.\end{aligned} \tag{20}$$

Thanks to the vector norms' properties, (20) can be reformulated as

$$\begin{aligned}\dot{\mathcal{V}} \le &-C\sum_i \left(1-\kappa_i|N_i|\right)\|\hat{z}_i\|^2 \\ &+\sum_i \left(1+\kappa_i|N_i| + C\vartheta_i|N_i|\right)\|\hat{z}_i\|\,\|\psi_i\| + C\sum_{i,j\in N_i}\kappa_j\|\hat{z}_i\|\,\|\hat{z}_j\| \\ &+C\sum_{i,j\in N_i}\vartheta_j\|\hat{z}_i\|\,\|w_j\| + \sum_i \vartheta_i|N_i|\,\|\psi_i\|^2 + \sum_{i,j\in N_i}\kappa_j\|\hat{z}_j\|\,\|\psi_i\| \\ &+\sum_{i,j\in N_i}\vartheta_j\|\psi_i\|\,\|w_j\| + \sum_{i,j\in N_i}(\varepsilon_i|N_i| + \varepsilon_j)\left(C\|\hat{z}_i\| + \|\psi_i\|\right).\end{aligned} \tag{21}$$

Now, by employing the Young's inequality feature as

$$xy \le (a/2)\,x^2 + (1/2a)\,y^2$$

for $a > 0$, (21) can be reformulated as

$$\begin{aligned}\dot{\mathcal{V}} \le &-C\sum_i \left(1-\kappa_i|N_i|\right)\|\hat{z}_i\|^2 + \sum_i \frac{a}{2}\left(1+\kappa_i + C\vartheta_i|N_i|\right)\|\hat{z}_i\|^2 \\ &+\sum_i \frac{1}{2a}\left(1+\kappa_i + C\vartheta_i|N_i|\right)\|\psi_i\|^2 \\ &+C\sum_{i,j\in N_i}\frac{a}{2}\kappa_j\|\hat{z}_i\|^2 + C\sum_{i,j\in N_i}\frac{1}{2a}\kappa_j\|\hat{z}_j\|^2 \\ &+C\sum_{i,j\in N_i}\frac{a}{2}\vartheta_j\|\hat{z}_i\|^2 + C\sum_{i,j\in N_i}\frac{1}{2a}\vartheta_j\|w_j\|^2 + \sum_i \vartheta_i|N_i|\,\|\psi_i\|^2 \\ &+\sum_{i,j\in N_i}\frac{a}{2}\kappa_j\|\hat{z}_j\|^2 + \sum_{i,j\in N_i}\frac{1}{2a}\kappa_j\|\psi_i\|^2 + \sum_{i,j\in N_i}\frac{a}{2}\vartheta_j\|\psi_i\|^2 \\ &+\sum_{i,j\in N_i}\frac{1}{2a}\vartheta_j\|w_j\|^2 + \sum_{i,j\in N_i}(\varepsilon_i|N_i| + \varepsilon_j)\left(C\|\hat{z}_i\| + \|\psi_i\|\right).\end{aligned} \tag{22}$$

Due to the symmetric graph of the communication layer, the indices in (22) can be used for each other. Therefore,

$$\begin{aligned}\dot{\mathcal{V}} \le &-\sum_i \left(C - \kappa_i C|N_i| - \frac{a}{2}\left(1+(\kappa_i + C\vartheta_i)|N_i|\right)\right)\|\hat{z}_i\|^2 \\ &+\sum_i \frac{1}{2a}\left(1+\kappa_i|N_i| + (2a+C)\vartheta_i|N_i|\right)\|\psi_i\|^2 \\ &+C\sum_{i,j\in N_i}\left(\frac{1}{2a}\left(\kappa_i a^2 + \kappa_i\right) + \frac{a}{2}(\vartheta_i + \kappa_i\frac{1}{C})\right)\|\hat{z}_i\|^2 \\ &+\sum_{i,j\in N_i}\left(\frac{1}{2a}\vartheta_i(C+1) + \frac{a}{2}\vartheta_i + \frac{1}{2a}\kappa_i\right)\|\psi_i\|^2 \\ &+\sum_{i,j\in N_i}(\varepsilon_i|N_i| + \varepsilon_j)\left(C\|\hat{z}_i\| + \|\psi_i\|\right).\end{aligned} \tag{23}$$

The arranged form of (23) can be represented by employing (??), as

$$\dot{\mathcal{V}} \leq -\sum_i (2Ca - \kappa_i(2a^2 + C(a+1)^2)\,|N_i| - a^2(1 + 2C\vartheta_i\,|N_i|))\frac{\|\hat{z}_i\|}{2a}$$
$$+ \sum_i \left(1 + 2\kappa_i + 2C\vartheta_i + \vartheta_i(a+1)^2\right)\frac{\|\psi_i\|^2}{2a}\,|N_i|$$
$$+ \sum_{i,j\in N_i} (\varepsilon_i\,|N_i| + \varepsilon_j)\left(C\,\|\hat{z}_i\| + \|\psi_i\|\right). \tag{24}$$

Due to this fact that a is always positive, the first two term of (24) can be negative as long as the following conditions being satisfied.

$$2Ca - a^2 - \kappa_i(2a^2 + (a+1)^2C)\,|N_i| - \vartheta_i(2Ca^2)\,|N_i| > 0 \tag{25}$$
$$1 + 2\kappa_i + \vartheta_i(2C + (a+1)^2) < 0 \tag{26}$$

To this end, the acceptable ranges for κ_i and ϑ_i can be determined through

$$0 < \vartheta_i < \frac{1 - a/2C}{a\,|N_i|}, \tag{27}$$
$$0 < \kappa_i < \frac{a/\,|N_i| - a^2(1+\vartheta_i)}{a^2(1 + 1/C) + a + 0.5} \tag{28}$$

in which, considering (27) for a valid selection of ϑ_i, a should be selected over $(0, 2C)$. Then, κ_i and ϑ_i can be easily tuned according to (27) and (28).

3.1.2. Zeno phenomenon

This phenomenon refers to a situation in control theory where an infinite number of events (or control updates) occur in a finite amount of time. It can lead to instability and impractical control implementations. Introducing a positive parameter in the ETM design, such as ε_i in (16), is a mechanism to prevent this phenomenon. This parameter typically represents a lower bound on the time between consecutive triggering events. In other words, it guarantees that triggering events do not occur too frequently, and preventing an infinite number of updates within a finite time interval. By having the positive lower bound such as ε_i in (16), the system avoids rapid and continuous triggering, mitigating the risk of the Zeno and maintaining stability.

To avoid happening this problem, a minimum time existence between two consecutive events entitled "inter-event time" is essential.

Considering the system described by (8) and the event-triggered mechanism (16). For any initial condition in $\mathbb{R}^N$, the defined inter-event time $\{t_{k+1} - t_k\}$ has a strictly positive lower bound. Unlike Shafiee et al. (2021), we demonstrate that the proposed event-triggered control strategy excludes the Zeno behavior through a novel solution. Firstly, we have

$$\frac{d}{dt}|\hat{x}_i(t) - x_i(t)| = -\frac{(\hat{x}_i(t) - x_i(t))\dot{x}_i(t)}{|\hat{x}_i(t) - x_i(t)|} \leq |\dot{x}_i(t)| \tag{29}$$
$$\leq |-\alpha(x_i(t) - v_{dci}) + \dot{v}_{dci} - \beta\sum_{j\in N_i} a_{ij}(\hat{x}_i(t) - \hat{x}_j(t))|$$
$$\leq |-\alpha\left(x_i(t) - \frac{1}{N}\sum_{j=1}^{N} v_{dci}\right) - \frac{\alpha}{N}\sum_{j=1}^{N} v_{dci} + \alpha v_{dci}|$$
$$+ |\dot{v}_{dci}| + \beta\sum_{j\in N_i} a_{ij}(|\tilde{e}_i| + |\tilde{e}_i| + 2\epsilon)|$$
$$\leq \alpha|\hat{x}_i(t) - x_i(t)| + \alpha(|\tilde{e}_i| + e_i) + |\frac{\alpha}{N}\sum_{j=1}^{N} v_{dci} + \alpha v_{dci}|$$
$$+ |\dot{v}_{dci}| + \beta\sum_{j\in N_i} a_{ij}(|\tilde{e}_i| + |\tilde{e}_i| + 2\epsilon)|$$

Considering $|e_i| \leq \|e\|$, $|v_{dci}| \leq k_1$ and $|\dot{v}_{dci}| \leq k_2$ where k_1 and k_2 are bounded constants, and defining $\bar{a}_i$ as the number of neighbors of ith DGU, we have

$$\frac{d}{dt}|\hat{x}_i(t) - x_i(t)| \leq \alpha|\hat{x}_i(t) - x_i(t)| + \sigma_i \tag{30}$$

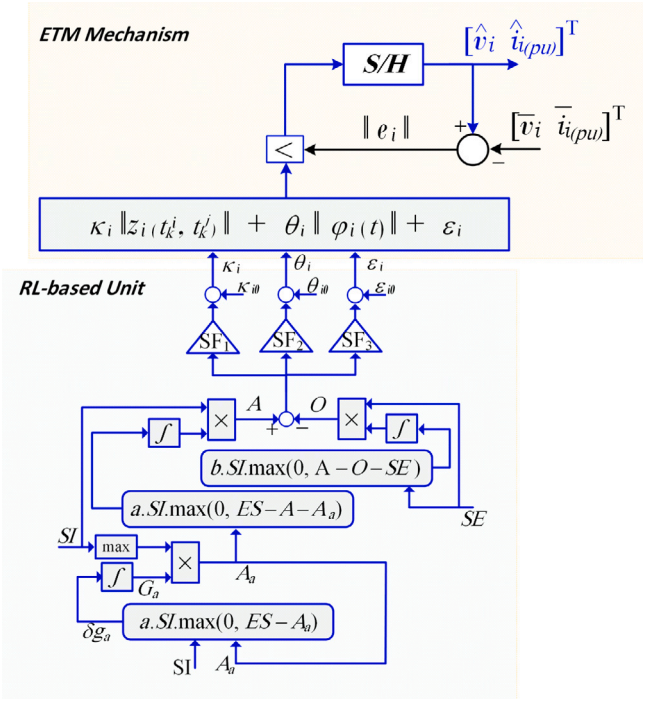

Fig. 3. Proposed intelligent reinforcement learning-based ETM.

in which $\sigma_i = (\alpha + 2\beta\bar{a}_i)\mathrm{Sup}(\|e\|) + |\frac{\alpha}{N}\sum_{j=1}^{N} k_1 + \alpha k_1| + k_2 + (\alpha + 2\beta\bar{a}_i)\varepsilon_i$. Regarding $\hat{x}_i(t) = x_i(t_i^k)$ and thanks to the Comparison Lemma (Khalil, 2002) yields

$$|\hat{x}_i(t) - x_i(t)| \leq \frac{\sigma_i}{\alpha}(e^{\alpha(t - t_k^i)} - 1). \tag{31}$$

Therefore, the time for the error of $|\hat{x}_i(t) - x_i(t)|$ to increase from 0 to ε_i is

$$\Delta t_i = t_{k+1}^i - t_k^i \geq \frac{1}{\alpha}\ln\left(\frac{\alpha\varepsilon_i}{\sigma_i} + 1\right). \tag{32}$$

Because of the positive constant value of Δt_i, the Zeno behavior does not exist.

Remark 1. As can be observed from (30), $|\hat{x}_i(t) - x_i(t)|$ has a direct relation with σ_i, and σ_i has a direct relation with ε_i; Consequently, increasing ε_i as Zeno condition threshold may degrade the steady state performance; However, from (32), it can be observed that the minimum interevent time Δt_i between two consecutive sequence becomes then larger, and therefore, the number of triggers can be reduced. Hence, a balance between control performance and signal transmission burden exists by an appropriate tuning of ε_i, and it can avoid Zeno phenomenon and keep the system stable.

3.2. Step II: Supplementary reinforcement learning-based gains design

The RL is used here for adaptive parameter tuning of ETM, since it provides a framework for learning more appropriate dynamic performance, while it can leads to reducing the number of event instants. The RL algorithm learns from interactions with the ETM controller and the consensus state variables used at ETM, leading to a better performance. The employed RL model is adaptable to changes in the environment. As the dynamics of the system vary, it can continuously adapt the ETM parameters to improve the system performance in the new conditions. Regarding the data source of the training model, the DGs as agents learn from interactions with the other DGs. The data source is the trajectory of consensus states, actions, and rewards experienced by the

agent during different types of disturbances like load changes (Batmani et al., 2022). Information about the current state of the DG voltage and LSH's status is utilized as the state data. The actions taken by the agent in response to the observed states for ensuring voltage regulation as shown by minimizing the performance index in (37) is utilized as the action data. And, the penalties associated with each action for ensuring appropriate load sharing, indicating the desirability of the agent's behavior as shown by the constraint term in (37), is utilized as the reward data.

The action step is generated through the integration of reward functions of the sensory inputs (SIs) and emotional signals (ESs). The functions representing SI and ES can generally be expressed in the forms as follows:

$$SI = \mathcal{F}(r, e, u, y) \tag{33}$$

$$ES = \mathcal{G}(r, e, u, y) \tag{34}$$

where the vector $r = [v_{ref}, i_o]$ is the vector of system inputs that correspond to the voltage DCA and current DCA, $e = [\delta v, \delta i]$ is the vector of consensus DCA voltage and consensus DCA current errors for SI, $u = [\bar{v}, \bar{i}]$ is the vector of the control inputs which contains the control inputs for ES, and $y = [\hat{v}, \hat{i}]$ is the vector of RL outputs.

By this way, the RL focuses on improving: (i) appropriate VR and LSH performance, (ii) and disturbance attenuation. Therefore, to achieve these goals, the corresponding SI and ES functions are designed as:

$$SI_i = K_1[v_{MG}(t) - \bar{v}_i(t)] + K_2 \int [\hat{v}_i(t) - \hat{v}_j(t)].dt \tag{35}$$

$$ES_i = K_3[\bar{i}_{i(pu)}(t) - i_{oi(pu)}(t)] + K_4 \int [\hat{i}_{i(pu)}(t) - \hat{i}_{j(pu)}(t)].dt \tag{36}$$

where the weighting factors K_1, K_2, K_3, and K_4, as in (35) and (36), can be determined by a training-based trial-error procedure, and for this paper they have been selected as $[K_1\ K_2\ K_3\ K_4]^T = [0.8\ 0.92\ 1.34\ 1.83]^T$. In addition, scaling factors (SFs) need to be considered in the output signals of the controllers to attain optimal results. Root mean square error can be a simple and effective way to appropriately tune of the SFs by minimizing the following performance index:

$$\min \quad OF = \sqrt{\int \left\| v_{MG} - \bar{v}_i(t) \right\|_2^2} \tag{37}$$

$$\text{Subject to:} \quad n_{di} i_{oi} = n_{dj} i_{oj} \qquad \forall i, j \in N$$

To analyze the stability of the system with the augmented RL-design, the methodology is extended to include a detailed explanation of the convergence condition.

Considering the characteristics of the proposed RL-based ETM on the SC into consideration, the stability of the proposed scheme depends on the conditions for asymptotic convergence of the outputs of A and O networks, considering the acceptable ranges in (33) and (28), and by recalling the following Theorem from Debnath and Mija (2020), we show the convergence conditions for the RL-based ETM design.

Theorem 1. *Considering the adjustment parameters a and b in Fig. 3, the following inequalities can be held for a combination of SI signals:*

$$(1)|1 - aSI(t)^2| < 1 \tag{38}$$

$$(2)|1 - bSI(t)^2| < 1 \tag{39}$$

which confirms the convergence of the weights of network A and network O asymptotically.

Proof. The dynamics of the controller can be considered through both the transient phase and steady-state phase. Specifically, within the transient phase, $\delta g(t)$ can be expressed as as shown by Fig. 3

$$\delta g(t) = \alpha \mathrm{SI}(t)[\mathrm{ES}(t) - A(t) - A_a(t)]. \tag{40}$$

While for the steady-state phase, one can consider that the variation of weights for both the A and O networks are zero. i.e.,

$$\delta g(t) = \delta g_a(t) = \delta h(t) = 0. \tag{41}$$

Applying the steady state conditions which lead to zero variation on the inputs of the integrators in Fig. 3 and assuming $\mathrm{SI}(t) \neq 0$ results in

$$\mathrm{ES}(t) = A_a(t) = \mathrm{SI}(t) G_a(t) = u(t). \tag{42}$$

Now, one can assume that g_a stands for the weight of network A during the adjustment procedure, and $\hat{g}_a$ and after the adjustment procedure; and considering that $\mathrm{ES}(t) = \mathrm{SI}(t)G_a(t)$ and $\hat{\mathrm{ES}} = \mathrm{SI}(t)G_a$ are the ES_i's signal before and after modification, respectively. The weight adjustment of δg_a can be written as follows:

$$\delta g_a(t) = a\mathrm{SI}(t)[\max(0, (\mathrm{ES}(t) - \hat{\mathrm{ES}}(t)))]. \tag{43}$$

In case of $\mathrm{ES} - \hat{\mathrm{ES}} \geq 0$, $\delta g_a(t)$ can be rewritten by the form

$$\begin{aligned} \delta g_a(t) &= a\mathrm{SI}(t)(\mathrm{ES}(t) - \hat{\mathrm{ES}}) \\ &= a\mathrm{SI}(t)\left(\mathrm{SI}(t)\hat{g}_a(t) - \mathrm{SI}(t)G_a(t)\right) \\ &= a\mathrm{SI}^2(t)\left(\hat{G}_a(t) - G_a(t)\right) \\ &= a\mathrm{SI}^2(t)\bar{G}_a(t) \end{aligned} \tag{44}$$

in which $\bar{G}_a(t) = \hat{G}_a(t) - G_a(t)$. Assuming small time-intervals δt, the changes of $G_a(t)$ can be formulated as

$$\begin{aligned} G_a(t + \delta t) &= G_a(t) + \delta g_a(t) \\ \bar{G}_a(t + \delta t) &= \hat{G}_a(t + \delta t) - G_a(t + \delta t) \\ &= \hat{G}_a(t + \delta t) - G_a(t) - \delta g_a(t) \\ &= \bar{G}_a(t) - a\mathrm{SI}^2\bar{G}_a(t) \\ &= (1 - a\mathrm{SI}^2)\bar{G}_a(t) \end{aligned} \tag{45}$$

In case of $|1 - a\mathrm{SI}^2| \prec 1$, $\bar{G}_a(t + \delta t)$ converges to $\hat{G}_a(t)$. By the same manner, the modification in Network O can be expressed as

$$\begin{aligned} \delta h(t) &= b\mathrm{SI}(t)(A(t) - O(t) - \mathrm{ES}(t)) \\ &= b\mathrm{SI}(t)\left(0 - \mathrm{SI}(t)H(t) - \mathrm{SI}(t)\hat{G}_a(t)\right) \\ &= -b\mathrm{SI}^2(t)\left(\hat{G}_a(t) + H(t)\right) \\ &= -b\mathrm{SI}^2(t)\bar{H}(t) \end{aligned} \tag{46}$$

where $\bar{H}(t) = \hat{G}a(t) + H(t)$. The variations for H(t) can be formed as

$$\begin{aligned} H(t + \delta t) &= H(t) + \delta h(t) \\ \bar{H}(t + \delta t) &= G_a^*(t + \delta t) + H(t + \delta t) \\ &= G_a^*(t + \delta t) + H(t) + \delta h(t) \\ &= \bar{H}(t) - bS^2\bar{H}(t) \\ &= (1 - b\mathrm{SI}^2)\bar{H}(t). \end{aligned} \tag{47}$$

As like as the convergence of $\bar{G}_a(t + \delta t)$, $\bar{H}(t + \delta t)$ converges to $\hat{H}(t)$ if $|1 - b\mathrm{SI}^2| \prec 1$. ■

4. Experimental results

To illustrate the merits of the ETM technique, a series of time-domain hardware in the loop (HIL) results are provided as shown by the equipments shown in Fig. 4. To do so, DGUs by output voltages 200 volt as shown in Fig. 4 with the listed parameters in Table 1 is connected to form a DC MG. The required parameters for the physical layer as well as the primary control layer is reported in Table 1. A Regatron DC power supply is used as the ideal energy storage supplier for all the DG units. 1.8 kW Danfoss inverters are used as the DC–DC boost converters for each DG unit. OPAL-RT simulator OP5600 as the target device is networked by a Lan cable with the host PC. The configuration of OP5600 includes four activated Intel Xeon E5, 3.2 GHz processing cores, which provides user-programmable I/O management, handled

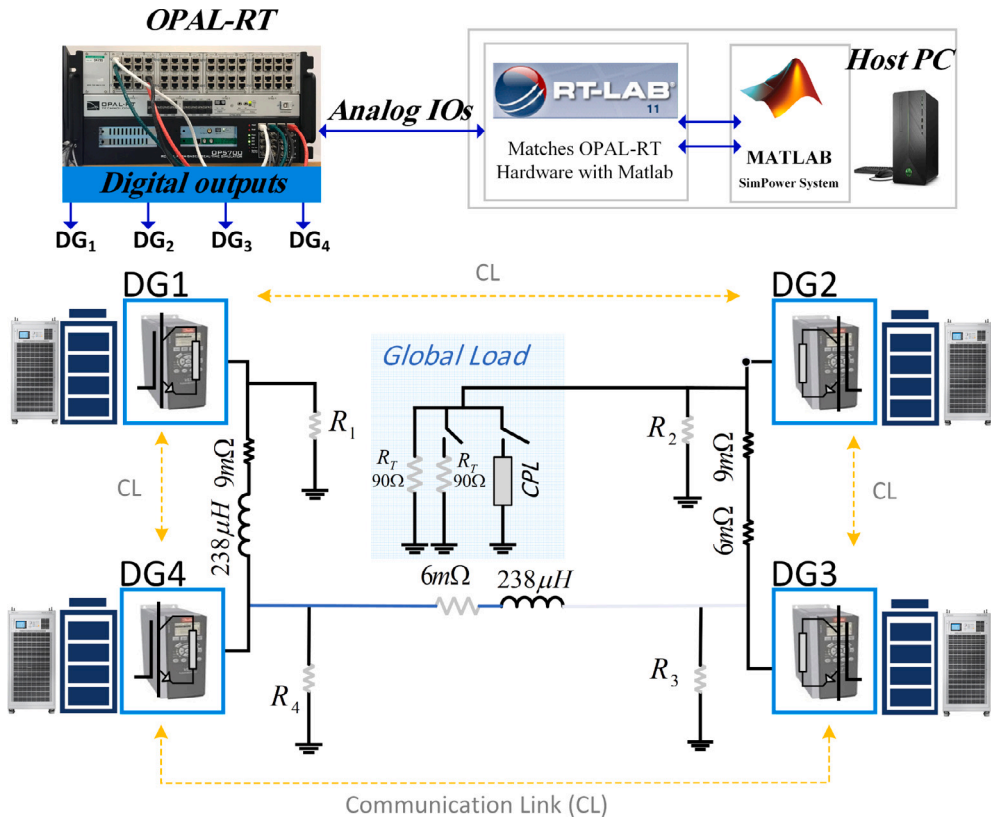

Fig. 4. Diagram of the considered MG.

Table 1
Electrical Configuration of the Studied DC Microgrid.

Description	DG 1	DG 2	DG 3	DGU 4
P_{rated} (kW)	0.9	1.8	0.9	1.8
Local load (W)	200	400	200	400
$n_d(\Omega)$	2	1	2	1
Voltage Controller's k_{pv}	4	4	4	4
Voltage Controller's k_{iv}	10	10	10	10
Current Controller's k_{pi}	30	30	30	30
Current Controller's k_{ii}	400	400	400	400

Table 2
Designed Parameters of the proposed RL-based ETM.

Description	DG 1	DG 2	DG 3	DGU 4
Voltage DCA's k_{pv}	1	1	1	1
Voltage DCA's k_{iv}	0.5	0.5	0.5	0.5
Current DCA's k_{pi}	1	1	1	1
Current DCA's k_{ii}	0.5	0.5	0.5	0.5
c_v	1	1	1	1
c_i	2	2	2	2
ϑ	0.1113	0.1176	0.1129	0.1132
κ	0.0407	0.0430	0.0389	0.0377
ε	0.0015	0.0015	0.0015	0.0015

by a fast Xilinx Spartan-3 FPGA used for digital outputs. RT-Lab code is then used for the Matlab codes for composing the C codes into OP5600.

Cyber layer configuration in the studied MG among whole the DGUs are also shown in Fig. 4, with dot-yellow double end arrows. For all DGUs, the design parameter $a = 1$ is considered for showing the weighted-communication links at the cyber layer. As mentioned before, positive values for c_v and c_i for the voltage and current DCAs should be considered, such that $c_v \geq 1$ and $c_i \geq 1$, as stated in (9) and (10). Their values for the design procedure are listed in Table 2, for each DGU. Accordingly, the stable range for ϑ and κ can be calculated as $\vartheta_i \in (0, 0.2380)$ and $\kappa_i \in (0, 0.04907)$, as stated before in (33) and (28). For all DGUs, a small positive scaler value for ε_i is selected as reported in Table 2. The communication bandwidth in the SC for data exchange is considered to have 300 Hz sampling time.

4.1. Scenario I: SC activation

In the first scenario, the performance of the proposed ETM is assessed for the studied MG; such that the MG operates merely by the drop mechanism before SC control activation. As it can be seen from Fig. 5, the studied MG is governed through the droop control mechanism when $t \in (0 - 1)$ s. During $t \in (0 - 1)$ s, there is a

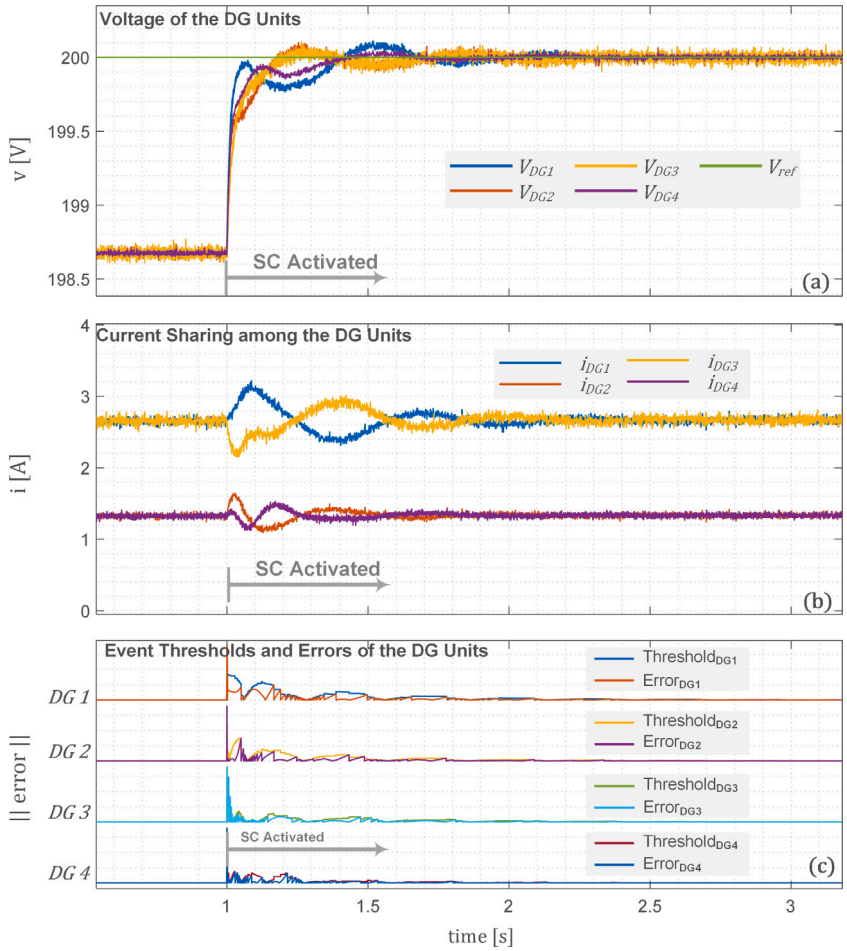

Fig. 5. The performance of the studied MG under Scenario I: SC activation (a) voltage of the units, (b) current sharing among the units, and (c) event thresholds and errors for all the units.

voltage deviation among the output voltage of DGUs and the reference value, and LSH is realized by the droop mechanism. At $t = 1$ s, the proposed RL-based ETM-based SC is activated, the voltage of each unit is regulated to the nominal voltage value as it is shown in Fig. 5(a), such that the current sharing is accurately insured after a transient as it is shown in Fig. 5(b). Fig. 5(c) shows the event thresholds and errors for all the units; whenever the error $e_i(t)$ passes its threshold, the S/H commands for exchanging required data in the communication layer.

4.2. Scenario II: Global load change

In this scenario, the proposed RL-based ETM technique is assessed during a constant power load change as the global load change. The constant power load can show a more serious case study for the current sharing assessing. To this end, at $t = 6$ s and at $t = 8$ s, the global constant power load is switched on and off such that the global load is changed from 0 to 800 Watt and then again to 0, respectively. During this scenario, not only the DGUs' voltage is appropriately restored (Fig. 6(a)), but accurate current sharing (Fig. 6(b)) are also attained. It can be observed that all the DGUs have participated in load sharing with respect to their nominal capacities and droop coefficients. The event thresholds and errors for all the units are shown in Fig. 6(c); the instants that the S/H commands for exchanging required data in the communication layer can be observed whenever the error $e_i(t)$ passes its threshold.

4.3. Scenario III: Plug-and-play capability

In this scenario, to assess the system performance during large transients is assessed by a DGU plug off and on. To this end, over the time interval $t \in [11 - 13]$ s, the DGU 4th is firstly plugged out and turned off from the MG. It can be observed from Fig. 7(a) that the voltage regulation is insured, however the 4th DGU is turned off and does not participate in load sharing as shown in Fig. 7(b); whereas other DGUs have increased and decreased their current sharing according to their nominal capacities and droop coefficients during plug-n-play time interval $t \in [11-13]$ s, respectively. As like as the previous scenarios, the event thresholds and errors for all the units are illustrated in Fig. 7(c); where the instants that the S/H commands for exchanging required data in the communication transmits, is shown whenever the errors $e_i(t)$ pass their thresholds.

4.4. Case study IV: Performance under partial line outage

In this case study, the performance of the proposed method under a partial line outage, as a line failure case study, is investigated. As it is shown in Fig. 8, a fault is happened in the connection line between DG1 and DG 2, and it limits most of the power contributed by DG 1 due to the high impedance line during faulty conditions.

In this case study, the considered partial line outage leads to about 90% reduction of the power contribution by DG 1. Before the partial line outage, there is no limitation for injecting the power by DG unit

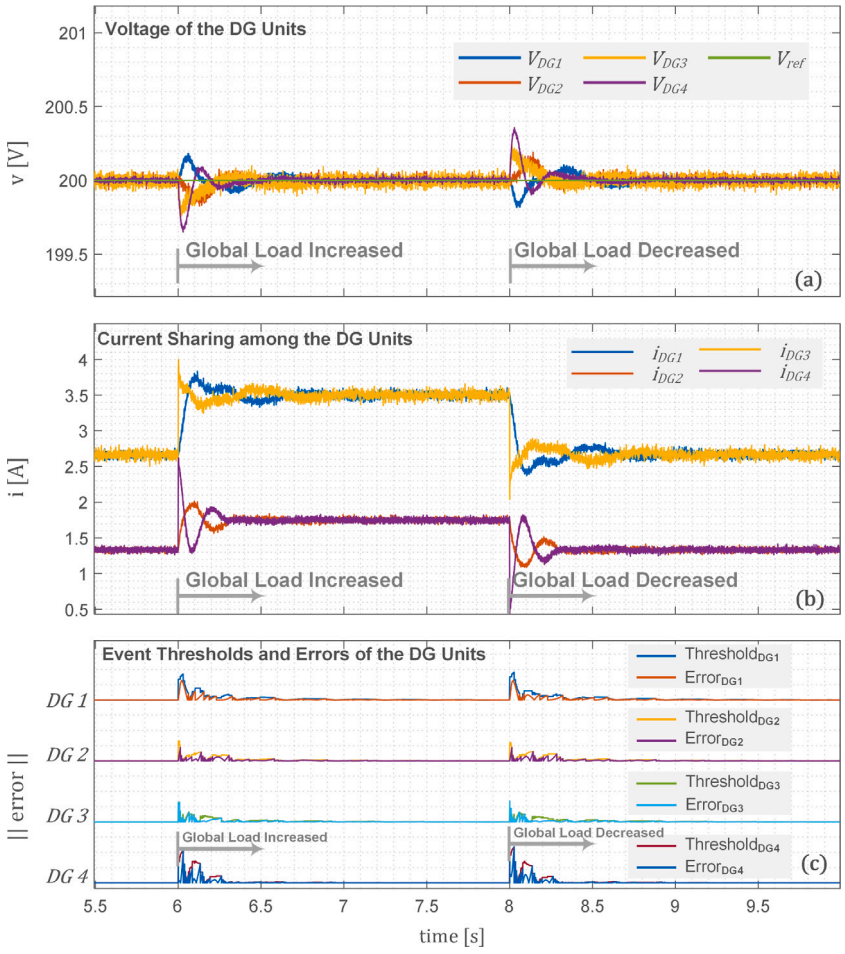

Fig. 6. The performance of the studied MG under Scenario II: Global Load Change: (a) voltage of the units, (b) current sharing among the units, and (c) event thresholds and errors for all the units.

1, while due to the high impedance of the related connection line during the partial line outage, and therefore, DG 1 cannot participate in power sharing appropriately, as the results confirm in Fig. 9. During this situation, *i.e.* $t \in [4-4.5]$, the required power by the global load is shared among the remained DG units properly. However event instants are increased among all the units, it leads to appropriate performance after fault clearance, both VR and LSH are satisfied, and system not only can keep its stability, but also provides an appropriate performance which confirms the validity of the proposed RL-based ETM scheme during the partial line failure.

4.5. Case study V: Comparison with other approaches

In order to highlight the merits and effectiveness of the proposed RL-based ETM technique with periodic time-trigger mechanism (P-TTM) and some recent ETM methods in Peng et al. (2020a), and Li et al. (2022) this scenario provides a comprehensive comparison among them. To exhibit the performance in a fairly comparing presentation, the trigger mechanism in Fig. 2 is merely replaced; it is then taken on that all the DGUs operate with a similar parameters for both of the physical, primary control level, and cyber-layer structures.

In order to perform this scenario, for the periodic time-trigger implementing, the ETM mechanism expressed in (16) is renewed by a 300 Hz S/H periodic sampling block, It is then renewed again with the ETM technique suggested in Peng et al. (2020a), and Li et al. (2022).

Now, a global load change is considered to assess the maximum overshoot, settling time, and the number of data exchanged among these techniques. The load is switched off and on at $t = 6$ s and $t = 8$ s, respectively. Fig. 11 elaborate the data exchanged pattern for all DG units in comparison with the number of exchanged information for the mentioned cases during $t \in [6-10]$ s. In addition, Table 3, shows maximum overshoot and settling time as the performance factors for a comprehensive investigation. Regarding Fig. ??, the minimum number data exchange is realized by utilizing the proposed RL-based ETM technique. In order to show the transferred data among the units with the proposed RL-based ETM technique and other ones, the numbers of data exchanged among units over the considered time slot are depicted in Fig. 11. The merits of the proposed RL-based ETM can be observed by the more reduced number of exchanged data compared with the periodic time-triggered and the existing methods in Peng et al. (2020a), and Li et al. (2022). In addition, both the maximum overshoot value and settling time show smaller values during the disturbance, which can confirm a better transient response can be provided by the proposed RL-based ETM in comparison with the other schemes.

To establish the effectiveness of our proposed RL-based ETM in reducing data communications compared to existing schemes, a comparison is done by focusing on the reduction of the communication data by triggering event instants. To this end, an experimental study to validate the performance of the proposed RL-based ETM is provided. This involves the comparison of event instants with existing schemes under a load change scenario to highlight the advantages of the RL-based ETM

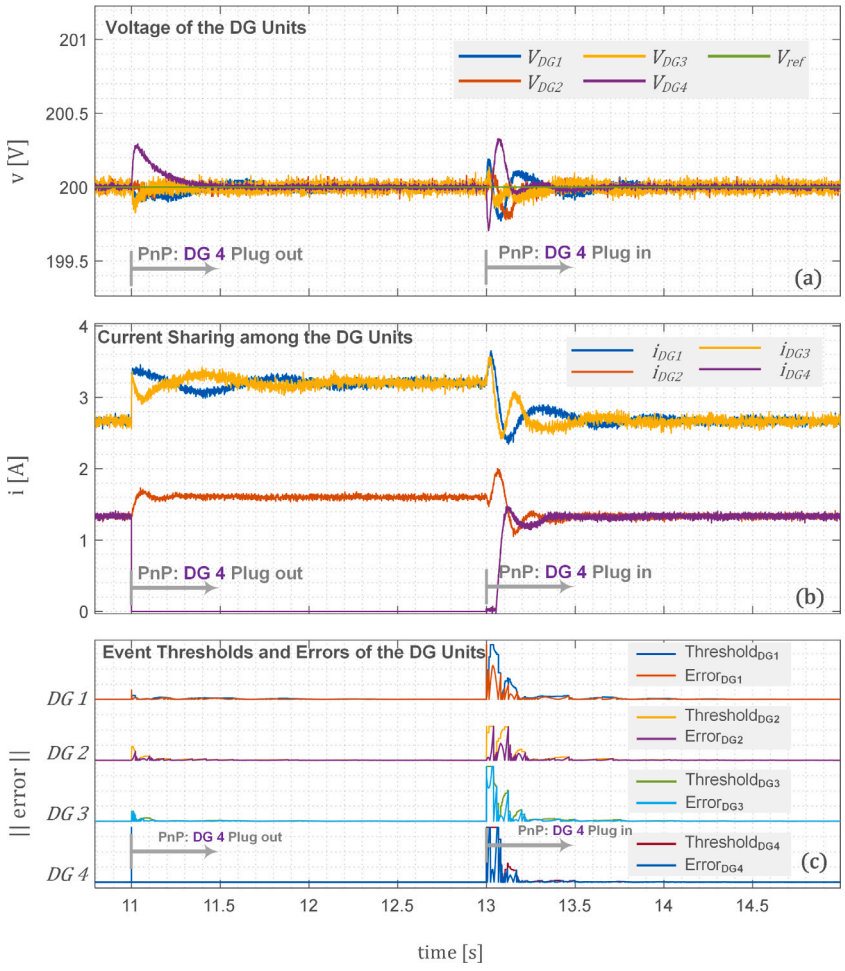

Fig. 7. The performance of the studied MG under Scenario III: Plug-and-Play Capability: (a) voltage of the units, (b) current sharing among the units, and (c) event thresholds and errors for all the units.

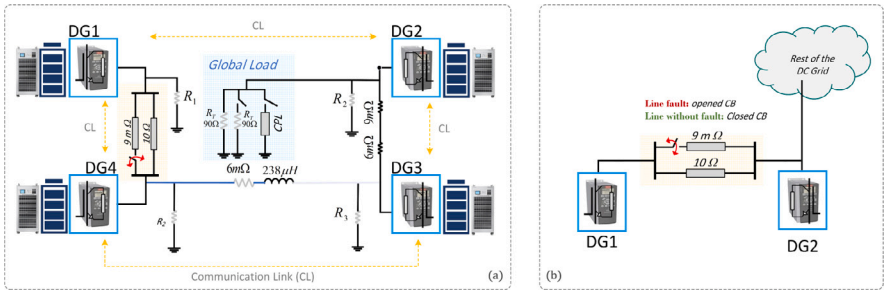

Fig. 8. Partial line outage as the line failure scenario to check the validity of the proposed scheme, (a) updated test system, and (b) partial line outage scenario to reduce the power flow out toward the global load as a faulty condition.

approach. In this scenario, quantitative results to clearly demonstrate the effectiveness of the RL-based ETM approach are illustrated. Fig. 10 shows the performance of the ETM scheme with and without the RL unit, where the last subfigure shows the number of event instants for each DG unit. As it can be seen, the RL-based ETM provides better dynamic performance for both the VR and LSH, while it uses fewer number of event instants, as a factor to show the effectiveness of the proposed RL-based ETM in reducing data communications than the conventional one.

4.6. Case study VI: performance during CI's time delays

To investigate the proposed RL-based ETM under cyber-layer uncertainties, the communication link between DGs 1st and 2nd is considered to exchange the information with time delays over the time interval $t \in [6-8]$ s. To assess the proposed RL-based ETM under CI delays, at $t = 6$ and $t = 8$ s, the global load power is also switched on and off, respectively; while communication delays are applied. As it can be recognized from Fig. 12, the performance for no delay, 400 ms delay, and 750 ms delay is depicted to show the VR, the LSH, and time instants. It can be seen that the RL-based ETM shows an appropriate performance for CI delays less than 400 ms, while it loses stability for CI delays higher than 750 ms.

5. Conclusion

The secondary control of DC MGs aims to eliminate voltage deviations while ensuring accurate and appropriate power sharing among all

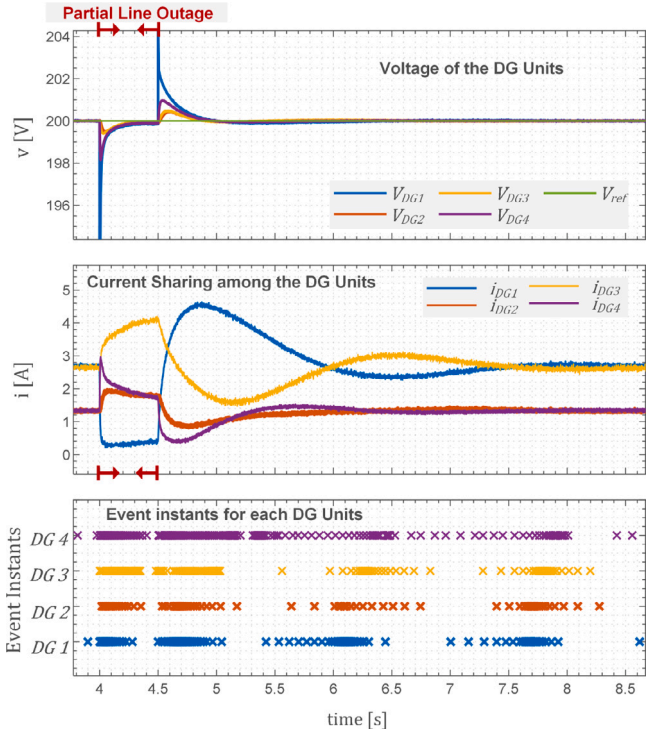

Fig. 9. Performance of the proposed RL-based ETM under a partial line outage scenario. From top to bottom, voltage of the DG units, current sharing among the DG units and event instants.

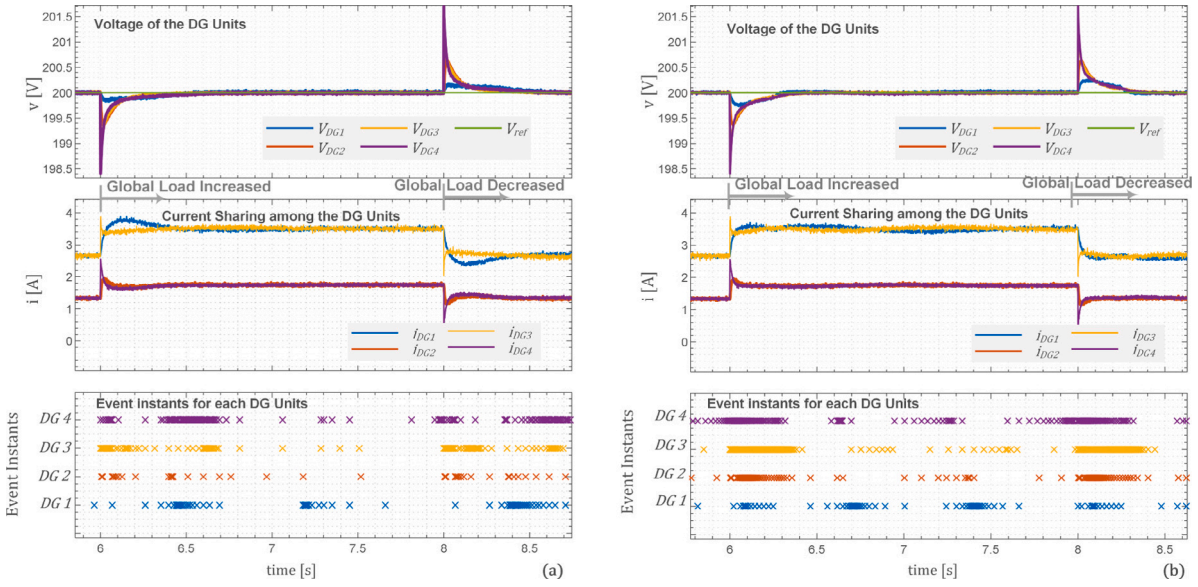

Fig. 10. Voltage regulation, current sharing among DG units, and event instants when: (a) the ETM scheme enhanced by the RL mechanism, and (b) the ETM scheme without the RL-based mechanism.

DGUs. To achieve these objectives, this paper presents a distributed reinforcement learning-based ETM, chosen for its reduced data-exchange requirements in the cyber layer and superior transient performance. The paper begins with a detailed modeling of DC MGs, followed by the design requirements for implementing an ETM that satisfies the SCL objectives. An adaptive reinforcement learning scheme for ETM parameters is then derived, employing a brain-emotional learning mechanism. The proposed RL-based ETM ensures that the current and voltage DCA converge to their nominal values. Comparative investigations show that the system exchanges fewer data among DGUs while maintaining

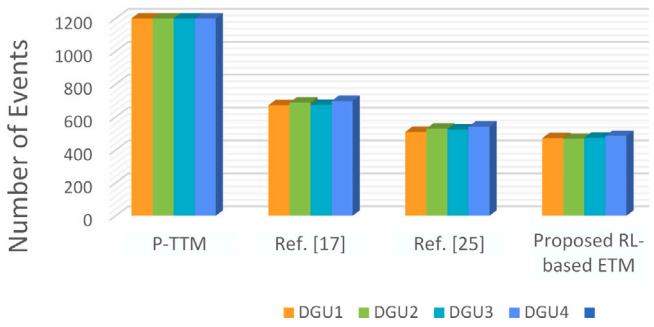

Fig. 11. Number of exchanged data for the proposed RL-based ETM technique in comparison with P-TTM communication, (Li et al., 2022), and (Peng et al., 2020a).

Table 3
Comparing the maximum overshoot and settling time of each DG unit with different ETM techniques in the SC layer.

		Maximum overshoot (%)				Settling time (ms)			
Method:		P- TTM	Li et al. (2022)	Peng et al. (2020a)	RL-ETM	P- TTM	Li et al. (2022)	Peng et al. (2020a)	RL-ETM
DG 1	v_{DG1}	8.06	9.23	6.42	0.0716	784	547	529	512
	i_{DG1}	34.1	38.4	47.3	23.1	1043	803	756	741
DG 2	v_{DG2}	10.03	9.17	8.60	0.042	813	627	593	581
	i_{DG2}	47.3	39.7	53.3	28.4	1013	847	815	784
DG 3	v_{DG3}	11.34	9.83	7.82	0.024	728	576	543	524
	i_{DG3}	52.4	43.2	64.1	21.1	1120	849	797	752
DG 4	v_{DG4}	12.07	10.26	9.13	0.0107	710	599	612	562
	i_{DG4}	68.3	45.27	73.1	14.7	970	909	798	719

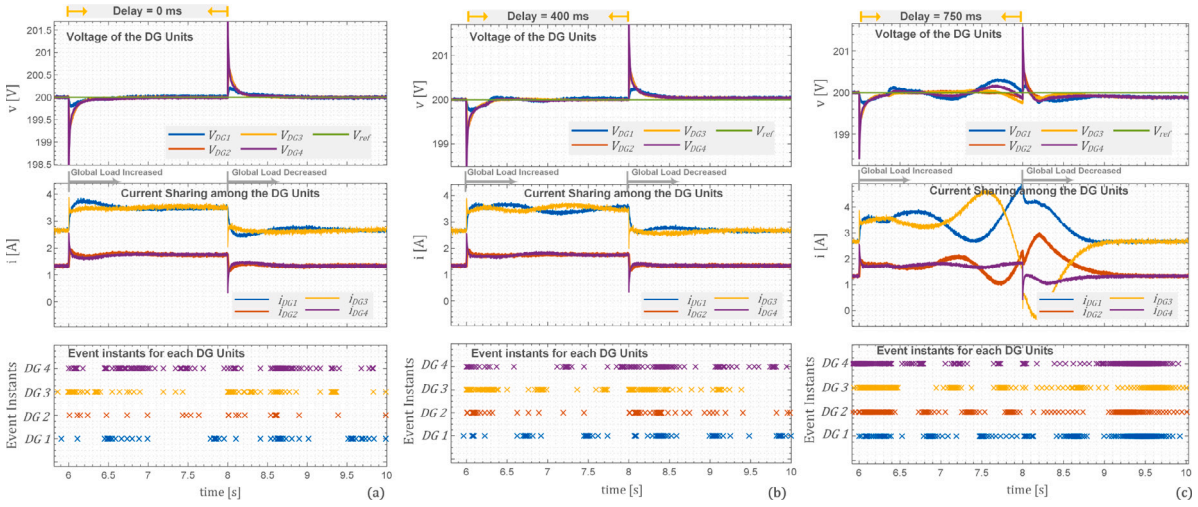

Fig. 12. Voltage regulation, current sharing among DG units, and event instants in the presence of CI delays: (a) when there is no communication delay, (b) when there is 100 ms communication delay, (c) when there is 750 ms communication delay, and system is loosing its LSH stability.

appropriate performance. It is also demonstrated that tuning design parameters can further reduce the communication burden. Finally, the effectiveness of the proposed RL-based ETM technique is validated through various experimental cases and a set of comparisons

CRediT authorship contribution statement

Houshmand Negahdar: Writing – original draft, Software, Methodology, Investigation, Conceptualization. **Amin Karimi:** Writing – original draft, Supervision, Software, Project administration, Methodology, Investigation, Conceptualization. **Yousef Khayat:** Writing – review & editing, Writing – original draft, Validation, Software, Investigation, Conceptualization. **Saeed Golestan:** Writing – review & editing, Writing – original draft, Supervision, Software, Methodology, Formal analysis, Conceptualization.

Declaration of competing interest

The authors declare that they have no known competing financial interests or personal relationships that could have appeared to influence the work reported in this paper.

Data availability

Data will be made available on request.

References

Afshari, A., Karrari, M., Baghaee, H.R., Gharehpetian, G.B., Guerrero, J.M., 2021. Robust cooperative control of isolated AC microgrids subject to unreliable communications: A low-gain feedback approach. IEEE Syst. J. 16 (1), 55–66.

Alavi, S.A., Mehran, K., Hao, Y., Rahimian, A., Mirsaeedi, H., Vahidinasab, V., 2018. A distributed event-triggered control strategy for DC microgrids based on publish-subscribe model over industrial wireless sensor networks. IEEE Trans. Smart Grid 10 (4), 4323–4337.

Ansari, S., Zhang, J., Singh, R.E., 2022. A review of stabilization methods for DCMG with CPL, the role of bandwidth limits and droop control. Protect. Control Mod. Power Syst. 7 (1), 2.

Barone, G., Buonomano, A., Forzano, C., Palombo, A., Russo, G., 2023. The role of energy communities in electricity grid balancing: A flexible tool for smart grid power distribution optimization. Renew. Sustain. Energy Rev. 187, 113742.

Batmani, Y., Khayat, Y., Salimi, A., Bevrani, H., Mirsaeidi, S., Konstantinou, C., 2022. SDRE-based primary control of DC microgrids equipped by a fault detection/isolation mechanism. Energy Rep. 8, 8215–8224.

Chen, L., Long, C., Li, Y., 2022. New solutions for smart grids with high-penetration distributed energy resources. Front. Energy Res. 9, 739253.

Debnath, B., Mija, S., 2020. Emotional learning based controller for quadruple tank system—An improved stimuli design for multiple set-point tracking. IEEE Trans. Ind. Electron. 68 (11), 11296–11308.

Du, S., Sheng, H., Sun, H.-Y., 2023. Fully distributed event-triggered consensus control for linear multiagent systems under DoS attacks. IET Control Theory Appl..

Fan, B., Peng, J., Yang, Q., Liu, W., 2019. Distributed periodic event-triggered algorithm for current sharing and voltage regulation in DC microgrids. IEEE Trans. Smart Grid 11 (1), 577–589.

Fathollahi, A., Gheisarnejad, M., Andresen, B., Farsizadeh, H., Khooban, M.-H., 2023. Robust artificial intelligence controller for stabilization of full-bridge converters feeding constant power loads. IEEE Trans. Circuits Syst. II.

Guo, F., Wang, L., Wen, C., Zhang, D., Xu, Q., 2019. Distributed voltage restoration and current sharing control in islanded DC microgrid systems without continuous communication. IEEE Trans. Ind. Electron. 67 (4), 3043–3053.

Jamali, M., Baghaee, H.R., Sadabadi, M.S., Gharehpetian, G.B., Anvari-Moghaddam, A., 2023. Distributed cooperative event-triggered control of cyber-physical AC microgrids subject to denial-of-service attacks. IEEE Trans. Smart Grid.

Khalil, H., 2002. Nonlinear Systems, third ed. Prentice-Hall, New Jersey.

Khalili, J., Dehkordi, N.M., Hamzeh, M., 2022. Distributed event-triggered secondary frequency control of islanded AC microgrids under cyber attacks with input time delay. Int. J. Electr. Power Energy Syst. 143, 108506.

Khayat, Y., Shafiee, Q., Heydari, R., Naderi, M., Dragičević, T., Simpson-Porco, J.W., Dörfler, F., Fathi, M., Blaabjerg, F., Guerrero, J.M., et al., 2019. On the secondary control architectures of AC microgrids: An overview. IEEE Trans. Power Electron. 35 (6), 6482–6500.

Li, L., Han, Y., Li, Q., Pu, Y., Sun, C., Chen, W., 2022. Event-triggered decentralized coordinated control method for economic operation of an islanded electric-hydrogen hybrid DC microgrid. J. Energy Storage 45, 103704.

Lu, J., Zhang, X., Zhang, B., Hou, X., Wang, P., 2021. Distributed dynamic event-triggered control for voltage restoration and current sharing in DC microgrids. IEEE Trans. Sustain. Energy 13 (1), 619–628.

Moradi, M., Heydari, M., Zarei, S.F., 2023. An overview on consensus-based distributed secondary control schemes in DC microgrids. Electr. Power Syst. Res. 225, 109870.

Moradi, M., Heydari, M., Zarei, S.F., Oshnoei, A., 2024. Discrete-time distributed secondary control of DC microgrids with communication delays. Electr. Power Syst. Res. 226, 109935.

Naderi, M., Khayat, Y., Shafiee, Q., Blaabjerg, F., Bevrani, H., 2023. Dynamic modeling, stability analysis and control of interconnected microgrids: A review. Appl. Energy 334, 120647.

Naderi, M., Khayat, Y., Shafiee, Q., Dragicevic, T., Bevrani, H., Blaabjerg, F., 2021. Comprehensive small-signal modeling and prony analysis-based validation of synchronous interconnected microgrids. Energy Rep. 7, 6677–6689.

Najafirad, M.J., Dehkordi, N.M., Hamzeh, M., Nazaripouya, H., 2023. Distributed event-triggered control of DC microgrids with input saturation and time delay constraints. IEEE Syst. J..

Nikoobakht, A., Aghaei, J., Mendes, G.P., Vahidinasab, V., 2022. Decentralized cooperation of natural gas and power systems with preserved privacy and decision-making independence. Renew. Sustain. Energy Rev. 168, 112855.

Peng, J., Fan, B., Yang, Q., Liu, W., 2020a. Distributed event-triggered control of DC microgrids. IEEE Syst. J..

Peng, J., Fan, B., Yang, Q., Liu, W., 2020b. Fully distributed discrete-time control of DC microgrids with ZIP loads. IEEE Syst. J..

Qian, Y.-Y., Wan, Y., Lin, Z., Shamash, Y.A., Davoudi, A., 2022. Distributed dynamic event-triggered control of power buffers in DC microgrids. IEEE Trans. Syst. Man Cybern.: Syst. 52 (12), 7748–7759.

Sepehrzad, R., Ghafourian, J., Hedayatnia, A., Al-Durrad, A., Khooban, M.H., 2023. Experimental and developed DC microgrid energy management integrated with battery energy storage based on multiple dynamic matrix model predictive control. J. Energy Storage 74, 109282.

Shafiee, P., Khayat, Y., Batmani, Y., Shafiee, Q., Guerrero, J.M., 2021. On the design of event-triggered consensus-based secondary control of DC microgrids. IEEE Trans. Power Syst. 37 (5), 3834–3846.

Shi, M., Shahidehpour, M., Zhou, Q., Chen, X., Wen, J., 2020. Optimal consensus-based event-triggered control strategy for resilient DC microgrids. IEEE Trans. Power Syst. 36 (3), 1807–1818.

Vafamand, N., Razavi-Far, R., Arefi, M.M., Saif, M., 2023. Fuzzy EKF-based intrusion detection and accurate state estimation of interconnected DC MGs with CPLs. IEEE Trans. Power Syst..

Wang, R., Sun, Q., Han, J., Zhou, J., Hu, W., Zhang, H., Wang, P., 2021a. Energy-management strategy of battery energy storage systems in DC microgrids: A distributed dynamic event-triggered H∞ consensus control. IEEE Trans. Syst. Man Cybern.: Syst. 52 (9), 5692–5701.

Wang, L., Xu, P., Qu, Z., Bo, X., Dong, Y., Zhang, Z., Li, Y., 2021b. Coordinated cyber-attack detection model of cyber-physical power system based on the operating state data link. Front. Energy Res. 9, 666130.

Wang, Y.-W., Zhang, Y., Liu, X.-K., Chen, X., 2024. Distributed predefined-time optimization and control for multi-bus DC microgrid. IEEE Trans. Power Syst..

Yan, S., Gu, Z., Ding, L., Park, J.H., Xie, X., 2023a. Weighted memory H_∞ stabilization of time-varying delayed Takagi-Sugeno fuzzy systems. IEEE Trans. Fuzzy Syst..

Yan, S., Gu, Z., Park, J.H., Xie, X., 2022. Sampled memory-event-triggered fuzzy load frequency control for wind power systems subject to outliers and transmission delays. IEEE Trans. Cybern..

Yan, S., Gu, Z., Park, J.H., Xie, X., 2023b. A delay-kernel-dependent approach to saturated control of linear systems with mixed delays. Automatica 152, 110984.

Zhou, J., Xu, Y., Sun, H., Wang, L., Chow, M.-Y., 2019. Distributed event-triggered H_∞ consensus based current sharing control of DC microgrids considering uncertainties. IEEE Trans. Ind. Inform. 16 (12), 7413–7425.